

## Electronic Supporting Information

# **Ab Initio Calculation of Magnetic Anisotropy and Thermal Spin Transition in the Variable Temperature Crystal Conformations of $[\text{Co}(\text{terpy})_2]^{2+}$**

Moromi Nath, Shalini Joshi, and Sabyashachi Mishra\*

*Department of Chemistry, Indian Institute of Technology Kharagpur, Kharagpur,  
India*

*\*Corresponding Author Email: [mishra@chem.iitkgp.ac.in](mailto:mishra@chem.iitkgp.ac.in)*

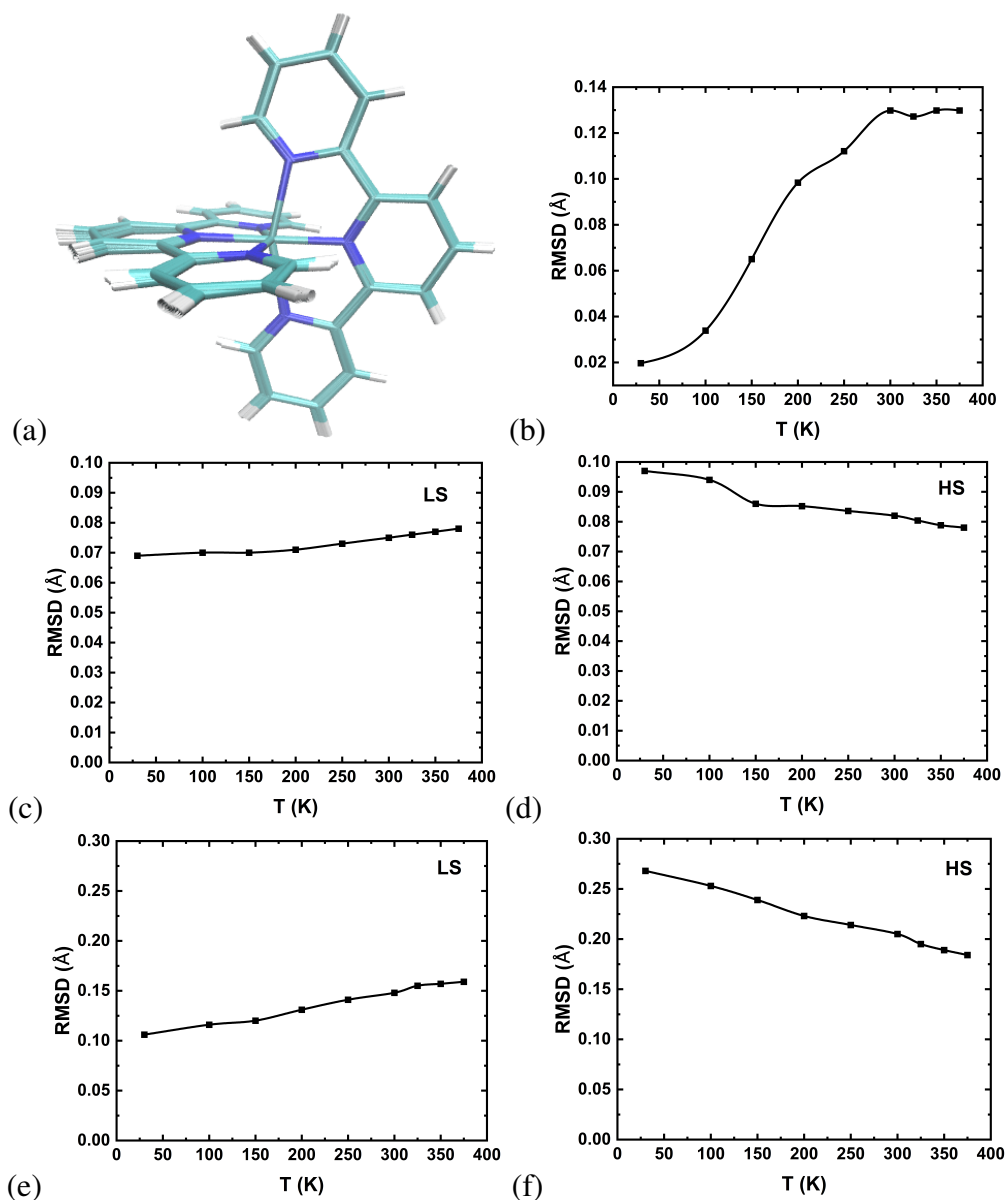


Figure S1: (a) The overlap of the crystal structures at nine different temperatures between 30 K to 375 K. (b) The RMSD of the crystal structures aligned with respect to the 30 K structure. (c) RMSD of the partially optimized structure in LS with respect to the corresponding X-ray crystal structure. (d) RMSD of the partially optimized structure in HS with respect to the corresponding X-ray crystal structure. (e) RMSD of the partially optimized structure with respect to the completely optimised structure in LS. (f) RMSD of the partially optimized structure with respect to the completely optimised structure in HS.

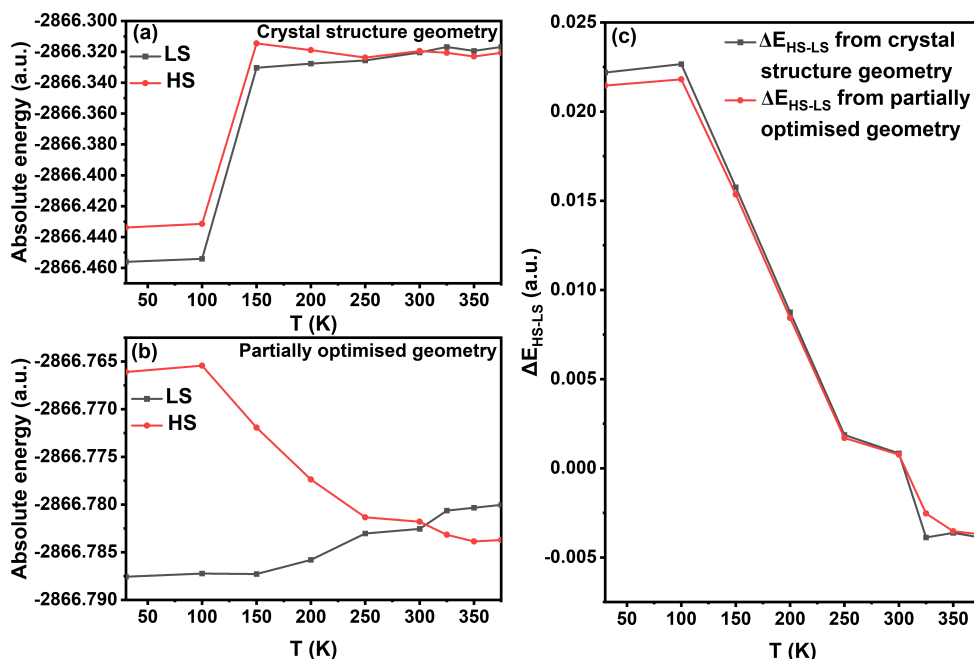


Figure S2: Potential energy of the complex (a) at crystal structures and (b) at partially optimised structures. (c)  $\Delta E_{HS-LS}$  from crystal structures and from partially optimised structures at different temperatures using B3LYP\* functional.

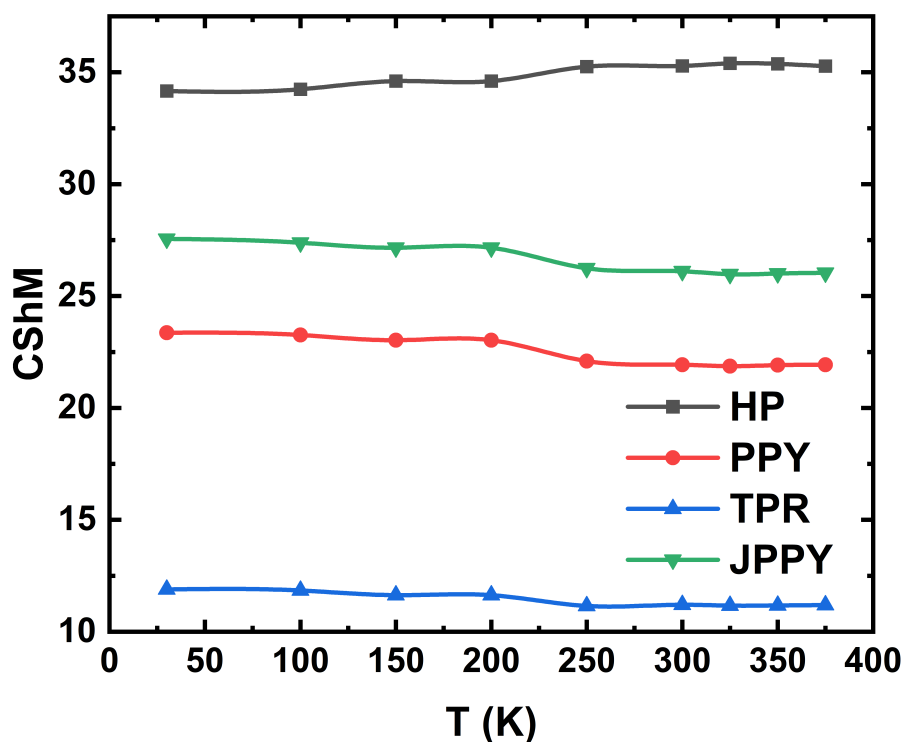


Figure S3: The continuous shape measure (CShM) map of the crystal structures at different temperatures with reference to different possible geometries in hexa-coordination: hexagon (HP), pentagonal pyramid (PPY), trigonal prism (TPR) and Johnson pentagonal pyramid (JPPY). The same with respect to the ideal octahedron is given in Figure 2(d) of the manuscript.

T (K)	$E_T$	$E_J$	$E_{Nuc}$	$E_V$	$E_X$	$E_C$
crystal structure geometries in LS						
30	2862.13	6058.14	4825.02	-16340.03	-260.58	-12.28
100	2861.99	6056.01	4822.88	-16335.66	-260.54	-12.27
150	2863.06	6047.41	4814.45	-16319.32	-260.78	-12.28
200	2863.21	6031.14	4798.08	-16286.79	-260.82	-12.28
250	2863.29	6013.36	4780.22	-16251.21	-260.84	-12.28
300	2863.08	5998.09	4764.84	-16220.40	-260.79	-12.28
325	2863.68	5997.61	4764.37	-16219.90	-260.93	-12.29
350	2863.47	5993.88	4760.61	-16212.26	-260.88	-12.28
375	2863.68	5997.61	4764.37	-16219.90	-260.93	-12.29
crystal structure geometries in HS						
30	2862.68	6057.98	4825.02	-16340.28	-260.71	-12.27
100	2862.55	6055.85	4822.88	-16335.92	-260.67	-12.27
150	2863.59	6047.22	4814.45	-16319.54	-260.91	-12.27
200	2863.72	6030.92	4798.08	-16286.95	-260.95	-12.27
250	2863.78	6013.11	4780.22	-16251.34	-260.97	-12.27
300	2863.56	5997.83	4764.84	-16220.51	-260.92	-12.27
325	2864.14	5997.32	4764.37	-16219.97	-261.05	-12.28
350	2863.94	5993.59	4760.61	-16212.33	-261.01	-12.27
375	2864.14	5997.32	4764.37	-16219.97	-261.05	-12.28
partially optimised geometries in LS						
30	2857.27	6045.28	4811.27	-16310.07	-259.43	-12.23
100	2857.30	6047.17	4813.18	-16313.90	-259.44	-12.23
150	2857.19	6029.82	4795.71	-16278.99	-259.42	-12.23
200	2857.09	6008.49	4774.26	-16236.14	-259.40	-12.22
250	2857.04	5989.53	4755.19	-16198.07	-259.39	-12.22
300	2857.04	5979.86	4745.48	-16178.68	-259.39	-12.22
325	2856.99	5973.87	4739.46	-16166.62	-259.38	-12.22
350	2856.96	5967.24	4732.79	-16153.30	-259.38	-12.22
375	2856.97	5967.57	4733.12	-16153.97	-259.38	-12.22
partially optimised geometries in HS						
30	2857.77	6044.14	4810.33	-16308.37	-259.55	-12.22
100	2857.81	6046.11	4812.32	-16312.36	-259.56	-12.22
150	2857.68	6028.80	4794.91	-16277.55	-259.54	-12.22
200	2857.56	6007.58	4773.59	-16234.92	-259.52	-12.22
250	2857.48	5988.68	4754.63	-16196.98	-259.51	-12.21
300	2857.48	5979.03	4744.96	-16177.67	-259.51	-12.21
325	2857.41	5973.09	4738.99	-16165.70	-259.49	-12.21
350	2857.38	5966.44	4732.31	-16152.34	-259.49	-12.21
375	2857.39	5966.79	4732.66	-16153.06	-259.49	-12.21

Table S1: Energy decomposition (in a.u.) of crystal structures (LS and HS) and partially optimised structures (LS and HS) at different temperatures using B3LYP\* functional in terms of kinetic energy ( $E_T$ ), Coulomb term ( $E_J$ ), nuclear-nuclear repulsion term ( $E_{Nuc}$ ), electron-nuclear attraction ( $E_V$ ), exchange term ( $E_X$ ) and correlation term ( $E_C$ ).

# 1 Calculation of the Gibbs Free Energies

The Gibbs free energy at a given temperature is expressed in terms of enthalpy ( $H$ ) and entropy  $S$  as,

$$G = H - TS_{\text{tot}}. \quad (\text{S1})$$

The enthalpy is given by the sum of the (internal energy  $E_{\text{tot}}$ ) and  $RT$ , with  $R$  as the universal gas constant. The total energy,  $E_{\text{tot}}$  is obtained as,

$$E_{\text{tot}} = E_{\text{opt}} + E_{\text{ZPE}} + E_{\text{thermal}}(T) \quad (\text{S2})$$

where  $E_{\text{opt}}$  is the optimized energy at the global minimum,  $E_{\text{ZPE}}$  is the zero-point energy, and  $E_{\text{thermal}}(T)$  is the thermal contribution to the total energy, obtained as<sup>1</sup>,

$$\begin{aligned} E_{\text{thermal}}(T) &= E_{\text{trans}} + E_{\text{rotation}} + E_{\text{vibration}} + E_{\text{electronic}} \\ &= \frac{3}{2}RT + \frac{3}{2}RT + R \sum_K \Theta_{\nu,K} \left( \frac{1}{2} + \frac{1}{e^{\Theta_{\nu,K}/T} - 1} \right) + RT^2 \left( \frac{\partial \ln q_{\text{el}}}{\partial T} \right)_V \end{aligned} \quad (\text{S3})$$

The total entropy,  $S_{\text{tot}} = R \left( \ln q_{\text{tot}} + T \left( \frac{\partial \ln q_{\text{tot}}}{\partial T} \right)_V \right)$ , can be expressed as the following sum of the translational, rotational, vibrational, and electronic entropies, i.e.,

$$\begin{aligned} S_{\text{tot}} &= R \left( \ln q_{\text{trans}} + \frac{5}{2} \right) + R \left( \ln q_{\text{rotation}} + \frac{3}{2} \right) + \\ &R \sum_K \left( \frac{\Theta_{\nu,K}/T}{e^{\Theta_{\nu,K}/T} - 1} - \ln(1 - e^{-\Theta_{\nu,K}/T}) \right) + R \left( \ln q_{\text{el}} + T \left( \frac{\partial \ln q_{\text{el}}}{\partial T} \right)_V \right), \end{aligned} \quad (\text{S4})$$

where the translational, rotational, and electronic partition functions are given by, respectively,

$$q_{\text{trans}} = \left( \frac{2\pi m k_B T}{h^2} \right)^{1/2} \frac{k_B T}{P} \quad (\text{S5})$$

$$q_{\text{rotation}} = \frac{\pi^{1/2}}{\sigma} \left( \frac{T^{3/2}}{(\Theta_x \Theta_y \Theta_z)^{1/2}} \right) \quad (\text{S6})$$

$$q_{\text{el}} = \omega_0 e^{-\epsilon_0/k_B T} + \omega_1 e^{-\epsilon_1/k_B T} + \omega_2 e^{-\epsilon_2/k_B T} + \dots \quad (\text{S7})$$

Here,  $m$  is the mass of the molecule,  $k_B$  is the Boltzmann constant,  $T$  is temperature,  $h$  is the Planck's constant,  $P$  is the pressure (1 atm considered),  $\sigma$  is the symmetry number (1 for the present complex),  $\Theta_x$ ,  $\Theta_y$  and  $\Theta_z$  are the rotational temperatures along the three principal axes of rotation, and  $\omega_i$  is the electronic degeneracy of the  $i$ th electronic state of energy  $\epsilon_i$ .

For a well-separated non-degenerate electronic ground state, the  $q_{\text{el}}$  reduces to the spin-degeneracy of the state. In the present case, since the ground quartet and ground doublet states show three- and two-fold quasi-degeneracy ( ${}^4T_{1g}$  and  ${}^2E_g$  in Oh geometry, respectively), we have included the contribution of the first three quartet and the first two doublet states in the evaluation of electronic partition function and electronic entropy. The vibrational temperatures are obtained from the normal harmonic vibrational frequencies at the globally optimised structures in LS and HS states for calculating vibrational entropy. To distinguish the low-frequency modes from internal-rotation modes, we used the so-called 'hindered-rotor' method during the harmonic vibrational analysis and calculation of different thermodynamic functions. For entropy calculation with different functionals, the rotational and vibrational temperatures were taken from the corresponding optimized geometries obtained with the concerned functionals. Figure S4 provides a comparison of the translational, rotational, vibrational, and electronic entropies of the LS and HS states at different temperatures. Among these, the vibrational entropy is found to provide the most dominant contribution.

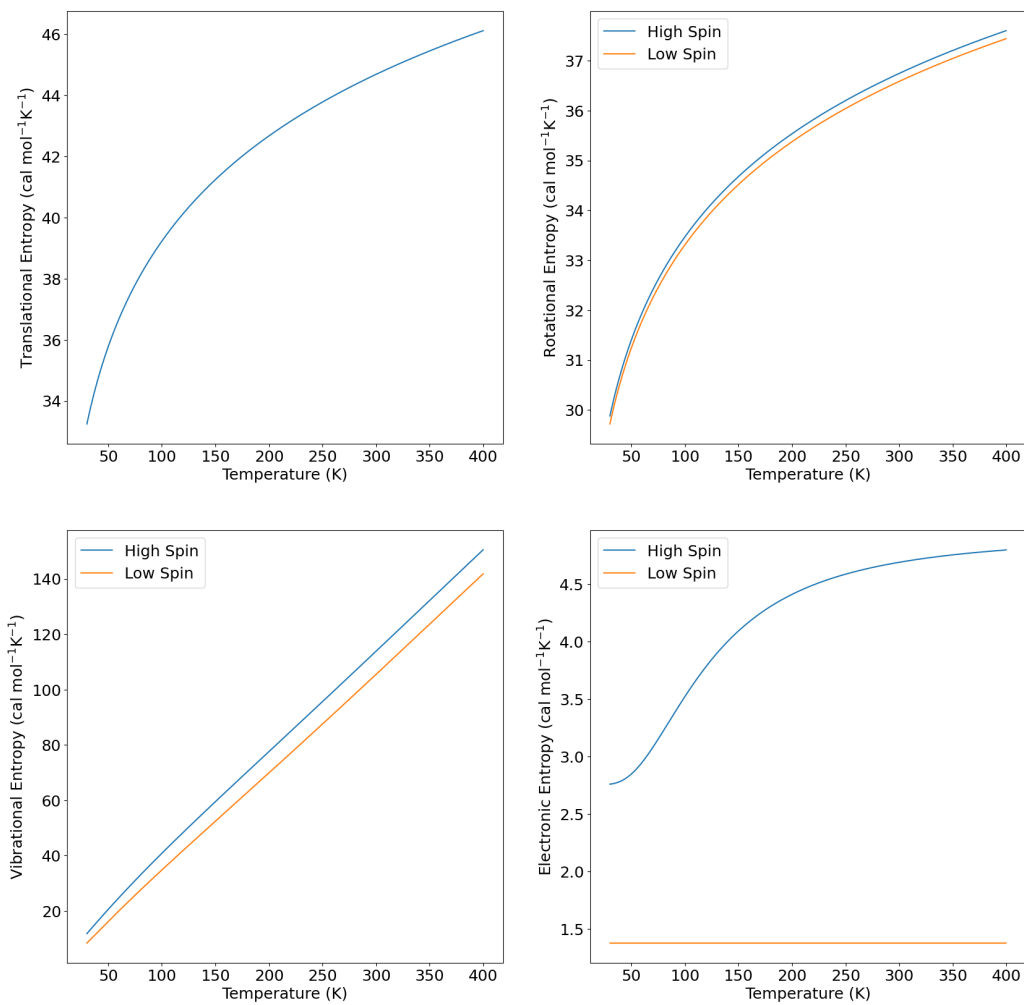


Figure S4: The (a) translational, (b) rotational, (c) vibrational, and (d) electronic entropies for HS and LS states at different temperatures obtained using B3LYP\* functional.

Table S2: NEVPT2 energies ( $\text{cm}^{-1}$ ) of the  ${}^2E_g$  and the  ${}^4T_{2g}$  states obtained from CAS(7, 5), CAS(7, 10), and CAS(11, 7) active spaces.

T (K)	CAS(7,5)		CAS(7,10)		CAS(11,7)	
	${}^2E_g$	${}^4T_{2g}$	${}^2E_g$	${}^4T_{2g}$	${}^2E_g$	${}^4T_{2g}$
30 K	0	0	0	0	0	0
	5586.2	963.8	5381.4	753.9	4949.6	440.0
100 K		1046.9		791.6		660.1
	0	0	0	0	0	0
	5522.0	743.8	4947.1	743.8	4840.0	263.9
150 K		826.9		826.7		330.0
	0	0	0	0	0	0
	4745.2	656.1	4781.3	656.3	4818.0	264.0
200 K		729.5		729.5		330.1
	0	0	0	0	0	0
	4088.5	566.7	4120.4	566.7	4813.6	219.9
250 K		695.6		695.6		330.0
	0	0	0	0	0	0
	3396.1	461.9	3422.7	462.0	4840.0	220.0
300 K		626.1		626.2		286.1
	0	0	0	0	0	0
	3798.1	419.5	3823.8	419.3	3943.5	220.2
325 K		573.3		573.3		383.9
	0	0	0	0	0	0
	3114.5	396.0	3138.7	396.2	3681.3	198.1
350 K		551.9		552.4		264.0
	0	0	0	0	0	0
	3200.34	362.8	3223.0	362.8	3505.9	176.0
375 K		520.1		520.1		247.3
	0	0	0	0	0	0
	3167.8	342.1	3168.0	342.1	3295.6	176.2
		518.9	518.9		242.0	

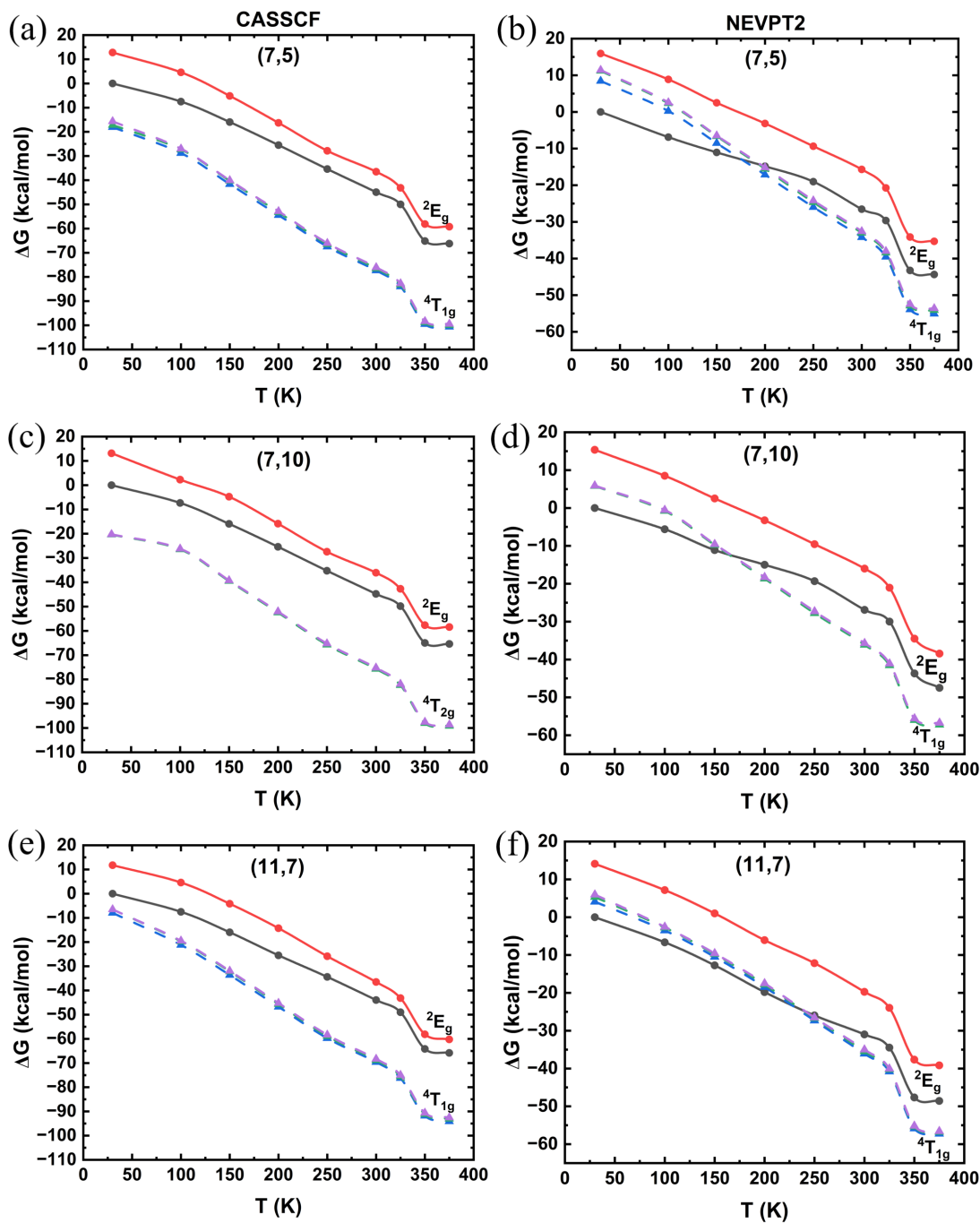
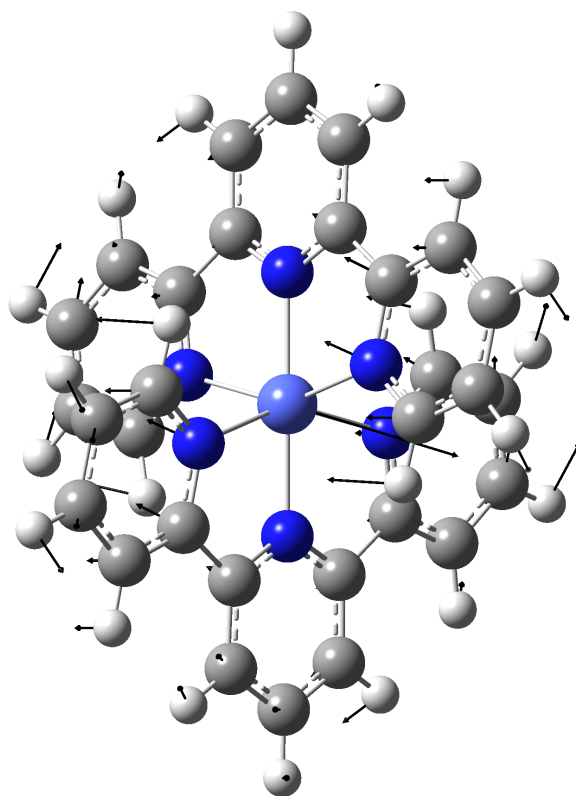
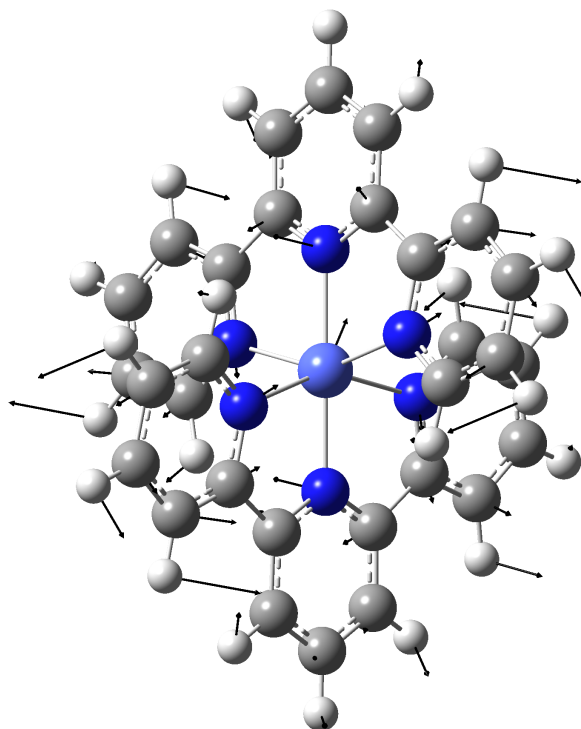


Figure S5: Gibbs free energy of the LS and HS ground states from CASSCF calculations (a,c,e) with active-space of (7,5), (7,10), and (11,7), respectively. The corresponding energy from NEVPT2 (b,d,f). All energies are shown relative to the LS ground state energy at 30 K structure. The HS states are shown by dashed lines, while the LS states by solid lines. The entropy contributions to the electronic energies are calculated (as mentioned in the previous section) using the required physical quantities from B3LYP\* functional. After including entropy corrections, the spin transition temperature estimated by NEVPT2 method reduces to 175 K for CAS(7,5), 150 K for CAS(7,10), and around 225 K for CAS(11,7). CAS(11,7) provides the best agreement with the experimentally observed spin transition temperature<sup>2</sup>

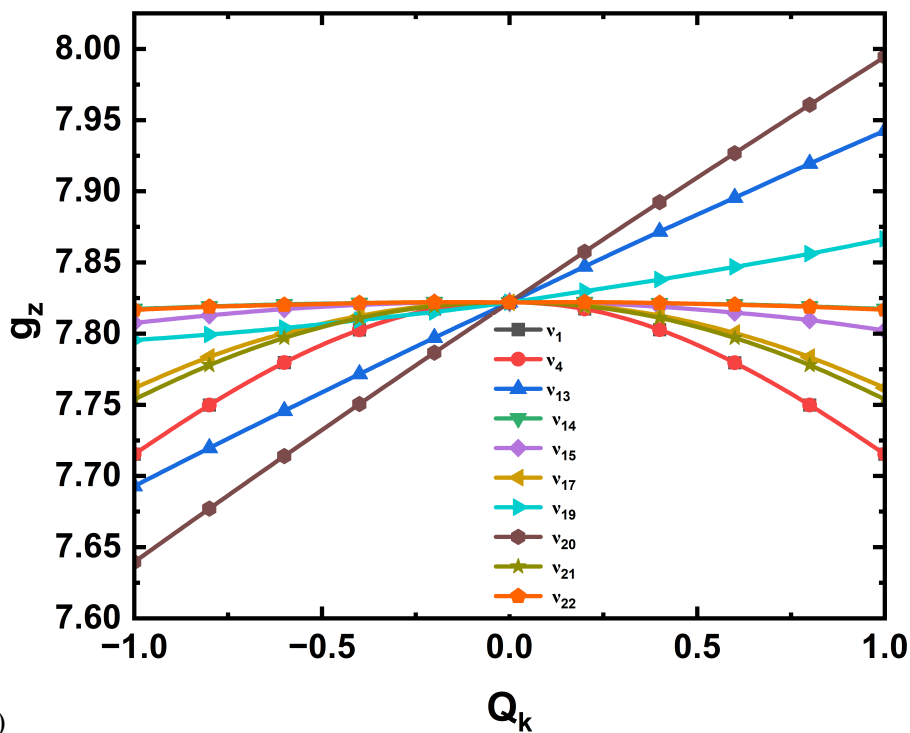


(a)

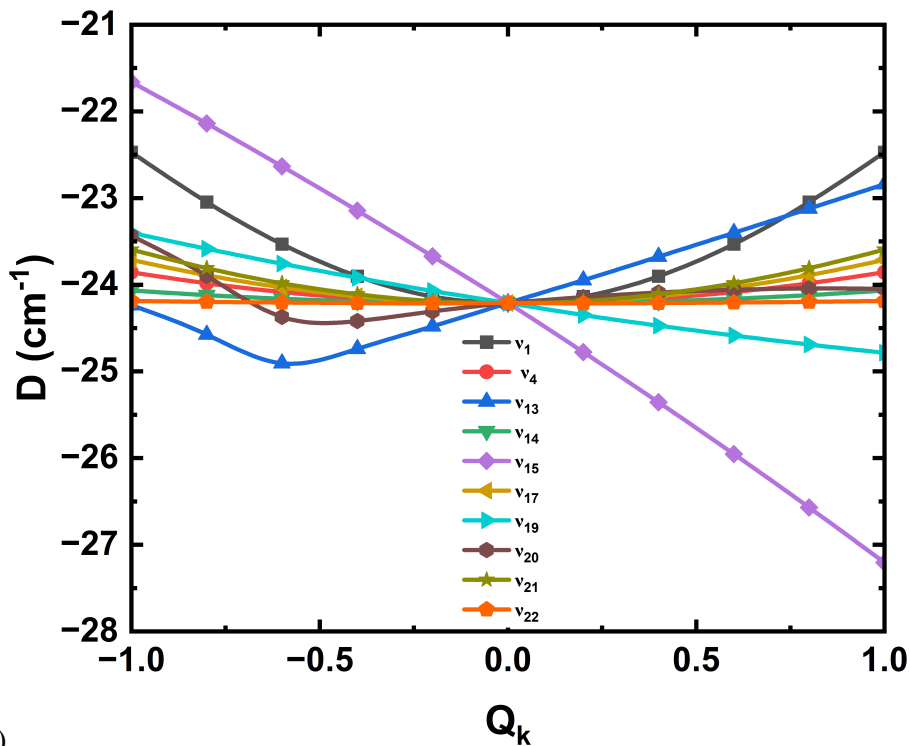


(b)

Figure S6: Normal modes of vibration along (a) mode 17 ( $205.11 \text{ cm}^{-1}$ ) and (b) mode 21 ( $233.56 \text{ cm}^{-1}$ ).



(a)



(b)

Figure S7: Variation of (a)  $g_z$  and (b)  $D$  for the selected vibrational modes along the dimensionless normal modes of vibrations.

Table S3: Matrix elements of the  $L_x$ ,  $L_y$ , and  $L_z$  operators with the d-orbitals basis<sup>3</sup>.

$L_x$	$ d_{z^2}\rangle$	$ d_{x^2-y^2}\rangle$	$ d_{xy}\rangle$	$ d_{yz}\rangle$	$ d_{zx}\rangle$
$ d_{z^2}\rangle$	0	0	0	$i\sqrt{3}$	0
$ d_{x^2-y^2}\rangle$	0	0	0	$i$	0
$ d_{xy}\rangle$	0	0	0	0	$-i$
$ d_{yz}\rangle$	$-i\sqrt{3}$	$-i$	0	0	0
$ d_{zx}\rangle$	0	0	$i$	0	0
$L_y$	$ d_{z^2}\rangle$	$ d_{x^2-y^2}\rangle$	$ d_{xy}\rangle$	$ d_{yz}\rangle$	$ d_{zx}\rangle$
$ d_{z^2}\rangle$	0	0	0	0	$-i\sqrt{3}$
$ d_{x^2-y^2}\rangle$	0	0	0	0	$i$
$ d_{xy}\rangle$	0	0	0	$i$	0
$ d_{yz}\rangle$	0	0	$-i$	0	0
$ d_{zx}\rangle$	$i\sqrt{3}$	$-i$	0	0	0
$L_z$	$ d_{z^2}\rangle$	$ d_{x^2-y^2}\rangle$	$ d_{xy}\rangle$	$ d_{yz}\rangle$	$ d_{zx}\rangle$
$ d_{z^2}\rangle$	0	0	0	0	0
$ d_{x^2-y^2}\rangle$	0	0	$-2i$	0	0
$ d_{xy}\rangle$	0	$2i$	0	0	0
$ d_{yz}\rangle$	0	0	0	0	$i$
$ d_{zx}\rangle$	0	0	0	$-i$	0

## References

- [1] D. A. McQuarrie, *Statistical Mechanics*, Harper Collins, New York, 1976.
- [2] C. A. Kilner and M. A. Halcrow, *Dalton Trans.*, 2010, **39**, 9008–9012.
- [3] O. Kahn, *Molecular Magnetism*, Courier Dover Publications, 2021